

Section 9: A Review of Indoor Localization Methods based on Inertial Sensors

Estefania Munoz Diaz, Dina Bousdar Ahmed and Susanna Kaiser

*German Aerospace Center (DLR),
Institute of Communications and Navigation,
Oberpfaffenhofen, 82234 Wessling, Germany.*

Abstract

Pedestrian navigation using inertial sensors constitutes an infrastructure-free positioning system. The fact that inertial sensors are already available in every smartphone or other carry on devices constitutes their great advantage and makes them especially interesting for mass market applications. This chapter offers a detailed explanation of the estimation of the orientation of the sensor, since it is of key importance in order to compute the position of the user. The positioning is usually derived in two different ways depending on the location of the sensor on the human body. These two approaches are deeply explained in this chapter. Disregarding the location on the human body where the sensor is mounted on, the accumulated drift error on the estimated positioning is an still unsolved issue using medium- and low-cost inertial sensors. The latest algorithms proposed to tackle the drift error are summarized in this chapter. Finally, an overview of the upcoming pedestrian inertial positioning is offered.

Keywords: Inertial sensors, orientation, strapdown, shoe-mounted, step&heading, step length, vertical displacement, drift, landmarks.

1. Introduction

Different solutions exist to solve the pedestrian indoor localization problem, but many of them rely on additional infrastructure that either needs to be installed or is assumed to be available. An overview of different techniques

5 that address the challenges in areas not covered by Global Navigation Satellite Systems (GNSS) is given in [1, 2, 3].

Radio and satellite navigation solve the positioning problem using the piloting method. Piloting is the process of determining one's position based on external objects, such as antennas or satellites. Inertial navigation performs po-
10 sitioning using the dead-reckoning method. Dead-reckoning is the process of determining one's current position projecting course and speed or elapsed distance from a known previous position. Dead-reckoning is, therefore an infrastructure-free positioning system.

Pedestrian dead-reckoning is performed using inertial sensors, that are usu-
15 ally combined with magnetometer and barometer. Inertial sensors are of high interest because of the possibility of providing positioning without touching privacy, unlike camera-based systems. Since medium- or low-cost inertial sensors are already available in every smartphone or other carry on electronic devices, the use of inertial sensors is especially interesting for mass market applications.

20 Example application areas suitable for inertial positioning are fire fighter rescuing, police men supervision, industrial inspections, or supervision of elderly people. Those professional applications require a system that is small-sized, light-weighted, has low power consumption, can be easily mounted on the body and is not dependent on infrastructure. For instance, in the case of fire, infras-
25 tructure might be disturbed. In addition, in some applications cameras might not be allowed as it is the case in industrial inspections. Integrating inertial sensors in clothes or footwear is an option to handle the fixation of sensors.

Suited sensor locations are the shoe or the pocket [4, 5]. Alternatively, sensor locations mounted e.g. at the wrist [6], at the head [7], at the torso [8] or in the
30 backpack are also investigated. Nevertheless, it is still challenging to use the sensors of the smartphones for positioning without any other help due the fact that the sensor is usually not fixed at the body and is in different motion mode like texting, phoning, swinging, or even in irregular motion mode [9].

Besides using only inertial sensors, fusion with other sensors or maps of
35 the environment [10, 11, 12, 13] is in any case possible and recommendable.

Additionally, the combination of sensors mounted on different locations of the human body is a promising solution for professional use cases [5].

In Section 2, inertial sensors as well as magnetometer sensors are explained. Pedestrian positioning systems based on inertial sensors are usually classified
40 depending on the location of the body where they are mounted on. This classification is based on the algorithm they use to compute the position of the pedestrian. There are two types of algorithms, namely strapdown and step&heading. These two algorithms correspond with shoe-mounted positioning systems and non-shoe-mounted positioning systems, respectively. The estimation of the ori-
45 entation is of key importance to perform inertial positioning and it is computed disregarding the location where the sensor is mounted on. Therefore, the orientation estimation is deeply described in Section 3, followed by the shoe-mounted inertial positioning in Section 4 and the non-shoe mounted inertial positioning in Section 5. The positioning estimation based on medium- and low-cost inertial
50 sensors suffers from propagation of errors and accumulated drift over time. Therefore, additional algorithms are necessary to compensate the drift. An extensive state of the art review is handled in Section 6. Finally, Section 7 is devoted to discussion of the present and future status of inertial positioning for pedestrians.

55 **2. Inertial Sensors and Magnetometers**

Inertial sensors are composed of accelerometers and gyroscopes, which measure specific force and turn rate, respectively. The so-called inertial measurement unit contains three mutually orthogonal accelerometers and three mutually orthogonal gyroscopes. Therefore, the acceleration and turn rate measurements
60 are triads.

Inertial sensors based on micro-electromechanical (MEMS) technology have improved its performance over the last decades. However, using MEMS-based inertial sensors the resulting positioning is less accurate than using other technologies like solid state accelerometers or optical gyroscopes [14]. The most

65 common error sources that disturb inertial measurements are biases, bias stability and thermo-mechanical noise [14].

The biases are the measured averaged value of the acceleration and turn rate when no acceleration nor rotation, respectively, is undergoing. The biases introduce a systematic error in the integrated measurements, i.e. velocity, position
70 and orientation. The systematic error can be compensated by averaging acceleration and turn rate while the sensor is static and subtracting the averaged value from the measured acceleration and turn rate, respectively.

The bias stability describes how the biases change over time under stable conditions, usually at constant temperature. Temperature fluctuations due to
75 changes in the environment and sensor self-heating modify the biases value. The change in the biases is caused by flicker noise, which is visible at low frequencies. Other slow changing errors affect also the bias values. The bias stability introduces a non-systematic error in the integrated signals due to the fact that the biases wander over time.

80 The thermo-mechanical noise introduces a white noise sequence, namely a sequence of zero-mean uncorrelated random variables. In turn, such a sequence disturbs the integrated measurements, i.e. velocity, position and orientation, by a random walk. A random walk is a process consisting of a series of steps, the direction and size of which are randomly determined [14].

85 Magnetometers, which are commonly embedded together with the inertial sensors, measure magnetic fields, e.g. the Earth's magnetic field. Usually, a magnetometer unit is formed by three mutually orthogonal magnetometers. MEMS-based magnetometers are frequently found in smartphones and similar electronic devices. Nevertheless, other technologies exist to implement magnetic
90 field sensors [15].

The main phenomenon that affects the performance of magnetic field sensors is the temperature effect. The temperature error causes an increasing noise present in the measured magnetic field. Therefore, temperature compensation algorithms or specific electronic design [16] are required to limit the temperature
95 effect.

For navigation purposes the Earth magnetic field is widespread used. However, magnetometers are also affected by the presence of ferromagnetic materials, which are common in urban and indoor environments. The modifications introduced by these materials lead to erroneous orientation estimation. This is the reason why magnetic field sensors are historically ruled out from indoor navigation systems. Nevertheless, magnetometers can still be used to improve the performance of inertial sensors [17, 18, 19].

3. Orientation Estimation

The orientation estimation aims at combining the measurements of gyroscopes, accelerometers and magnetometers in an optimal way to obtain the orientation of the sensor. Along with the orientation angles, it is convenient to estimate also the biases of the gyroscopes. The biases, which were explained in Section 2, are therefore estimated in order to be subtracted from the turn rate measurements.

A common tool to compute the orientation in the state of the art is the Kalman filter. A Kalman filter is one implementation of Bayesian filters used to estimate the states of a system. In the particular case of the orientation estimation the states are the orientation angles, i.e. ϕ roll, θ pitch and ψ yaw or heading, and the biases of the gyroscope.

The Kalman filter combines a prediction stage and an update stage. The prediction stage implements the system model, which represents how the system states evolve over time. The update stage incorporates measurements that relate to the system states. Usually the prediction stage is based on the integration over time of the turn rate measurements. The update stage typically incorporates the acceleration and magnetic measurements in order to reduce the error due to the integration over time of the turn rate measurements that contain biases and noise.

Both, the full state and the error state Kalman filter have similar performance, as shown in [20]. In this chapter, the full state vector is chosen, being

\mathbf{x}_o^k composed of the orientation angles and the biases \mathbf{b}^k of the gyroscopes:

$$\mathbf{x}_o^k = [\phi^k, \theta^k, \psi^k, b_x^k, b_y^k, b_z^k]^T. \quad (1)$$

In the following, α, ω, μ will be used to represent acceleration, turn rate and magnetic measurements, respectively.

125 3.1. Prediction Stage

Gyroscopes measure in body frame the turn rate of the sensor with respect to the inertial frame. In order to have the turn rate measurements in body frame with respect to the navigation frame, the transport rate and the Earth rotation have to be subtracted. However, for pedestrian positioning, the transport rate
 130 is negligible and the Earth rotation, which is approximately 15° h^{-1} , is usually not compensated. Therefore, it is assumed that the turn rate measured by the gyroscopes is approximately the turn rate of the sensor in body frame with respect to the navigation frame (see Figure 1).

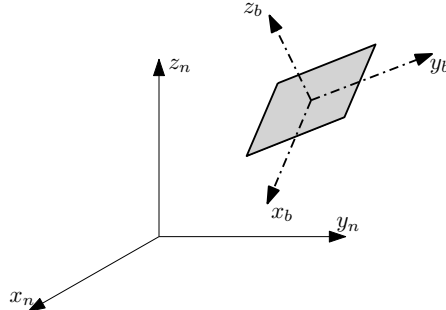


Figure 1: Navigation frame, $\{x, y, z\}_n$, and body frame of the sensor, $\{x, y, z\}_b$. The navigation frame is fixed over time. The body frame changes with the sensor orientation.

The turn rate at the time k is defined as $\boldsymbol{\omega}^k = [\omega_x^k, \omega_y^k, \omega_z^k]^T$. To compute
 135 the orientation, the biases have to be subtracted from the turn rate. Then, the corrected turn rate measurements are integrated once over time.

The direction cosine matrix \mathbf{C}^k is a 3×3 matrix in which each column is a unit vector along the body axes specified in terms of the navigation axes. That means, the matrix \mathbf{C}^k represents the rotation of the body frame with respect

140 to the navigation frame at the time k (see Figure 1). From this rotation the orientation of the sensor is deduced.

The orientation at the time k is the orientation at the time $k-1$ modified by the rotation that took place within the last δt seconds, represented in a matrix form as \mathbf{A}^k :

$$\mathbf{C}^k = \mathbf{C}^{k-1} \cdot \mathbf{A}^k, \quad (2)$$

being \mathbf{A}^k

$$\mathbf{A}^k = \mathbf{I} + \frac{\sin(\sigma)}{\sigma} \cdot \mathbf{B}^k + \frac{1 - \cos(\sigma)}{\sigma^2} \cdot \mathbf{B}^{k2}, \quad (3)$$

where $\sigma = |\boldsymbol{\omega}^k \delta t|$ and

$$\mathbf{B}^k = \begin{pmatrix} 0 & -\omega_z^k \delta t & \omega_y^k \delta t \\ \omega_z^k \delta t & 0 & -\omega_x^k \delta t \\ -\omega_y^k \delta t & \omega_x^k \delta t & 0 \end{pmatrix}. \quad (4)$$

In order to tackle the estimation of the biases of the gyroscope, a noise model is presented in the following. The biases are predicted using the presented model. The turn rate measurements $\boldsymbol{\omega}^k$ can be represented as

$$\boldsymbol{\omega}^k = \tilde{\boldsymbol{\omega}}^k + \mathbf{e}^k, \quad (5)$$

being $\tilde{\boldsymbol{\omega}}^k$ the error free turn rate and \mathbf{e}^k the measurement error. The turn rate error can be decomposed into two errors

$$\mathbf{e}^k = \mathbf{b}^k + \boldsymbol{\nu}, \quad (6)$$

where $\boldsymbol{\nu}$ is the sensor noise that can be modelled as Gaussian white noise. To determine the biases error an auto-regressive model of order one (AR1) [21] is chosen. The AR1 model is defined as

$$\hat{\mathbf{b}}^k = \mathbf{c} \cdot \mathbf{b}^{k-1} + \mathbf{n}. \quad (7)$$

The biases follow an exponentially correlated noise term defined in the AR1 model as the constant \mathbf{c} , which is equal to the term $e^{-\frac{1}{\tau}}$, where τ is the correlation coefficient for each axis and \mathbf{n} can be modelled as Gaussian white noise
 145 with standard deviation $\sigma_{\mathbf{n}}$ for each axis.

3.2. Update Stage

There are several updates that can be implemented to improve the orientation estimation. Usually the updates are signals directly measured by the sensors, but also pseudo-measurements can act as updates. The term pseudo-measurement refers to non-directly measured but computed signals. In the following, the most important updates will be summarized.

3.2.1. Absolute Gravity Update

During the walk, there are periods in which the acceleration due to the movement of the sensor is zero or quasi-zero. During these periods only the gravity acceleration is measured. In such case, the orientation angles roll and pitch can be extracted at the time k as follows:

$$\bar{\phi}^k = \arctan\left(\frac{\alpha_y^k}{\alpha_z^k}\right) \quad (8)$$

and

$$\bar{\theta}^k = \arctan\left(\frac{-\alpha_x^k}{\sqrt{\alpha_y^{k2} + \alpha_z^{k2}}}\right). \quad (9)$$

The measurement vector \mathbf{z}_o^k of the Kalman filter at the time k can be written as:

$$\mathbf{z}_o^k = [\bar{\phi}^k, \bar{\theta}^k]^T. \quad (10)$$

3.2.2. Differential Gravity Update

Likewise, within the periods of zero or quasi-zero acceleration, the acceleration at the current time can be computed applying the rotation of the last δt seconds, \mathbf{A}^k , to the acceleration measured at the previous time α^{k-1} as follows:

$$\bar{\alpha}^k = \mathbf{A}^k \cdot \alpha^{k-1}. \quad (11)$$

The pseudo-measurement $\bar{\alpha}^k$ is used as update. This update has been proposed in [22]. The measurement vector \mathbf{z}_o^k of the Kalman filter at the time k can be written as:

$$\mathbf{z}_o^k = [\bar{\alpha}_x^k, \bar{\alpha}_y^k, \bar{\alpha}_z^k]^T. \quad (12)$$

3.2.3. Absolute Magnetic Field Update

During the walk there are periods in which the measured magnetic field is constant or quasi-constant. At the beginning of the quasi-constant magnetic field period, the measured magnetic field is projected onto the navigation frame and chosen as reference $\bar{\boldsymbol{\mu}}_r$. It is assumed that, during quasi-constant magnetic field periods, the measured magnetic field does not change. Therefore, the reference magnetic field is used as pseudo-measurement for the update. This update has been proposed in [17] and further analyzed in [23]. The measurement vector \mathbf{z}_o^k of the Kalman filter at the time k can be written as:

$$\mathbf{z}_o^k = [\bar{\mu}_{rx}, \bar{\mu}_{ry}, \bar{\mu}_{rz}]^T. \quad (13)$$

155 3.2.4. Differential Magnetic Field Update

Likewise, within these periods of constant or quasi-constant magnetic field, the magnetic field at the current time can be computed applying the rotation of the last δt seconds, \mathbf{A}^k , to the magnetic field measured at the previous time $\boldsymbol{\mu}^{k-1}$ as follows:

$$\bar{\boldsymbol{\mu}}^k = \mathbf{A}^k \cdot \boldsymbol{\mu}^{k-1}. \quad (14)$$

The pseudo-measurement $\bar{\boldsymbol{\mu}}^k$ is used as update. This update has been proposed in [18] and [17]. The measurement vector \mathbf{z}_o^k of the Kalman filter at the time k can be written as:

$$\mathbf{z}_o^k = [\bar{\mu}_x^k, \bar{\mu}_y^k, \bar{\mu}_z^k]^T. \quad (15)$$

3.2.5. Absolute Compass Update

If the measured magnetic field is homogeneous, the yaw angle can be computed at each time k as follows:

$$\bar{\psi}^k = \arctan\left(\frac{-\mu_{hx}^k}{\mu_{hy}^k}\right) + D, \quad (16)$$

being μ_{hi}^k where $i = \{x,y\}$ is the magnetic field intensity at the time k for the i -axis projected onto the horizontal plane. The declination angle, which is

known for every location on the Earth, is represented by D . The measurement z_o^k of the Kalman filter at the time k can be written as:

$$z_o^k = \bar{\psi}^k. \quad (17)$$

3.2.6. Zero Angular Rate Update

Within the periods where the sensor is not rotating, the turn rate measurements can be assumed to be zero. This assumption implies that any turn rate measured during these periods is due to errors, e.g. biases. This update has been proposed in [24]. The measurement vector z_o^k of the Kalman filter at the time k can be written as:

$$z_o^k = [0, 0, 0]^T. \quad (18)$$

4. Shoe-Mounted Inertial Positioning

Shoe-mounted positioning systems represent the first massively implemented positioning system for pedestrians. Shoe-mounted positioning is usually derived with the strapdown algorithm. The biomechanics of the foot allow performing re-calibrations at every step, thus limiting the rapidly growing positioning error. Back in 2005, Foxlin [25] proposed to re-calibrate the strapdown algorithm for shoe-mounted systems performing Zero-velocity UPdaTes (ZUPT).

The strapdown algorithm is composed of two phases, namely orientation estimation and position estimation. Figure 2 represents the block diagram of the strapdown algorithm

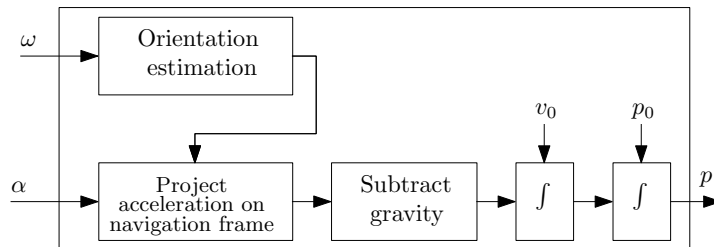


Figure 2: Block diagram of the strapdown algorithm.

The orientation estimation is performed as explained in Section 3, resulting in a direction cosine matrix \mathbf{C}^k that represents the rotation of the body frame with respect to the navigation frame for each time k . The position estimation phase starts after the orientation is computed. The orientation is used to project the acceleration measurements onto the navigation frame.

$$\boldsymbol{\alpha}_n^k = \mathbf{C}^k \cdot \boldsymbol{\alpha}^k. \quad (19)$$

Secondly, the gravity acceleration, $\mathbf{g}_n = [0, 0, g]^T$, is subtracted from the projected acceleration. By doing so, the remaining acceleration corresponds only to the acceleration due to the movement of the body. Lastly, this remaining acceleration is integrated twice over time to compute the position. The algorithm strapdown requires an initial position p_0 , an initial velocity v_0 and also an initial orientation. This is represented in the following equations:

$$\mathbf{v}_n^k = \mathbf{v}_n^{k-1} + \delta t \cdot (\boldsymbol{\alpha}_n^k - \mathbf{g}_n), \quad (20)$$

and

$$\mathbf{p}_n^k = \mathbf{p}_n^{k-1} + \delta t \cdot \mathbf{v}_n^k, \quad (21)$$

being \mathbf{p}^k the position at the time k , \mathbf{v} the velocity at the time k and δt the sampling time.

The shoe-mounted positioning is usually implemented using a Kalman filter, whose state vector \mathbf{x}_p is defined as follows:

$$\mathbf{x}_p^k = [\mathbf{p}^k, \mathbf{v}^k, \boldsymbol{\Psi}^k, \mathbf{b}^k]^T, \quad (22)$$

170 being $\boldsymbol{\Psi}^k$ the orientation at the time k and \mathbf{b}^k the biases of the gyroscope at the time k . Also an error state Kalman filter is possible. The Kalman filter for shoe-mounted positioning systems is divided into two stages namely prediction and update. The equations described above represented by the block diagram of Figure 2 represents the prediction stage. For error state Kalman filters, the
 175 equations described above do not form part of the filter, since the states consist of errors.

The aforementioned re-calibrations are performed during the update stage. The human gait cycle comprises eight phases [26]. Four of them can be observed using a foot-mounted sensor, i.e. the loading response, mid-stance, terminal stance and swing as shown in Figure 3.

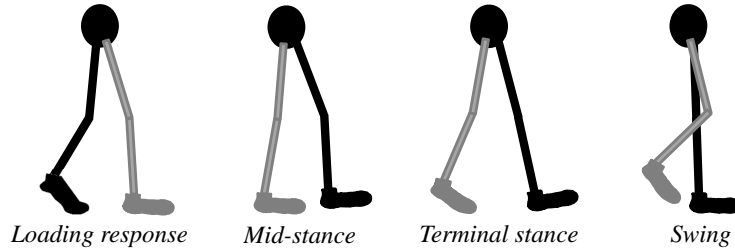


Figure 3: Diagram of the gait phases visible using inertial sensors mounted on the right shoe (grey leg).

180

In the case of shoe-mounted inertial positioning, the mid-stance is of high interest. The mid-stance phase is the period of the gait cycle when the foot is in contact with the ground. Figure 4 represents the vertical acceleration measured by a shoe-mounted accelerometer. During the stance phases, indicated by the shadowed areas, the only acceleration measured by the shoe-mounted accelerometers is the gravity. Constant acceleration implies zero velocity, thus ZUPT corrections can be applied during these periods.

185

The stance phase detection is usually performed based on thresholds for the acceleration and turn rate [25]. If both the acceleration and turn rate are within predefined thresholds during a minimum time, the stance phase is detected. The authors in [27] developed a stance phase detection based on a finite-state machine. In the latter, each phase of the human gait is a state of the finite-state machine. Such an approach can even detect the foot stance phase in challenging situations like walking the stairs.

190

Stance phase detection algorithms however, require these thresholds to be adapted to the particular inertial sensors, to the pedestrian or both. Furthermore, threshold-based algorithms perform optimally during walking on flat surfaces. In order to detect stance phases during other activities, e.g. walking

195

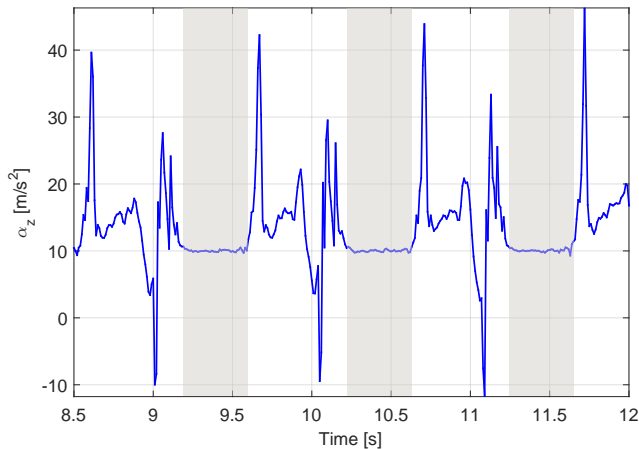


Figure 4: Vertical acceleration measured by shoe-mounted accelerometers during three steps. The shadowed areas indicate the time when the foot is in mid-stance phase.

stairs, a more sophisticated method is suggested by the authors in [27]. The
 200 disadvantage of the latter is its complexity regarding both, design and imple-
 mentation.

Upon detection of the stance phase, the states of the filter are updated with
 the ZUPT pseudo-measurement vector z_p^k at the time k that can be written
 as:

$$z_p^k = [0, 0, 0]^T. \quad (23)$$

The use of ZUPT pseudo-measurements makes the error growth linear in
 time instead of cubic. The error accumulation, although linear, remains a chal-
 lenge in pedestrian positioning based on shoe-mounted inertial sensors.

205 5. Non-Shoe-Mounted Inertial Positioning

Non-shoe-mounted positioning systems are of high interest, because they
 can make use of the inertial sensors embedded in any wearable such as smart
 watch, smart glasses and smart clothing among others. The error accumulated
 using these sensors cannot be mitigated with zero-velocity corrections, since the
 210 targeted body locations i.e. head, wrist... continuously move while walking.

Therefore, in these cases the step&heading algorithm, represented in the block diagram of Figure 5, is appropriate.

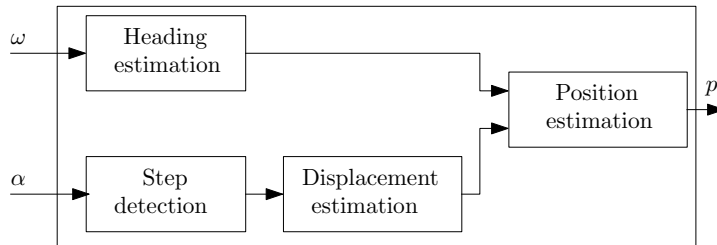


Figure 5: Block diagram of the step&heading algorithm.

The step&heading algorithm is based on the following equations:

$$\begin{aligned} p_x^k &= p_x^{k-1} + s^k \cdot \cos(\psi^k), \\ p_y^k &= p_y^{k-1} + s^k \cdot \sin(\psi^k), \end{aligned} \quad (24)$$

where p_x^k and p_y^k represent the position in the x- and y-axis at the time k , s^k stands for the step length at the time k and ψ^k is the heading of the pedestrian
 215 at the time k . Therefore, in order to compute the position of the pedestrian, two steps are necessary: the orientation estimation, to have the heading angle, and the displacement estimation.

The orientation estimation is carried out as described in Section 3. The different updates are not usually applied continuously, but only within particular periods, as explained in Section 3. From the complete orientation, usually
 220 only the heading angle ψ is used to compute the position of the pedestrian, as indicated in Equation (24).

The step&heading algorithm is usually defined in 2D, as indicated in Equation (24). However, for particular sensor locations it is possible to solve 3D positioning. In that case the position in the z-axis is as follows:

$$p_z^k = p_z^{k-1} + d_z^k, \quad (25)$$

where d_z^k represents the vertical displacement from the time $k - 1$ to the time k . The authors in [28] demonstrate that, if the inertial sensors are attached to

225 the lower limb of the pedestrian, it is possible to differentiate between walking horizontally and climbing stairs by means of the orientation of the leg of the pedestrian. The information on the walking surface allows deriving the vertical displacement d_z .

The displacement estimation, being the step length or also the vertical displacement, is triggered every time a new step is detected, as shown in Figure 5. 230 The following subsections detail the step detection on horizontal surfaces, the step detection on stairs, the step length estimation and last but not least the vertical displacement estimation.

5.1. Step Detection on Horizontal Surfaces

235 The well known algorithm to detect steps is based on acceleration measurements. This algorithm is valid for all sensor locations. Figure 6 shows the acceleration measured with the sensor introduced in the front pocket of the trousers. The dashed curve represents the norm of the acceleration $\|\alpha\|$ where the gravity has already been subtracted. A common procedure is to apply a low-pass filter (LPF) to this signal, in order to improve the performance regarding undetected steps and false detected steps. The LPF curve is shown 240 in solid blue and the detected steps are highlighted with black sticks. In [29], the performance of step detectors based on the norm of the acceleration and its low-pass filtered version has been analyzed. For horizontal surfaces, i.e. 2D walks, the false step detection rate decreases by using the filtered acceleration. 245

For some sensor locations, e.g. the lower limb, the step detection can also be performed using the pitch angle estimation, as suggested in [28, 30]. Figure 7 shows the pitch angle estimation for seven steps where the sensor has been introduced in the front pocket of the trousers. The detected steps are highlighted 250 with black sticks. In [29], the performance of the step detector based on the pitch has been compared with the step detector based on the acceleration. The authors demonstrate that the step detection based on the pitch angle is more robust also for different walking speeds.

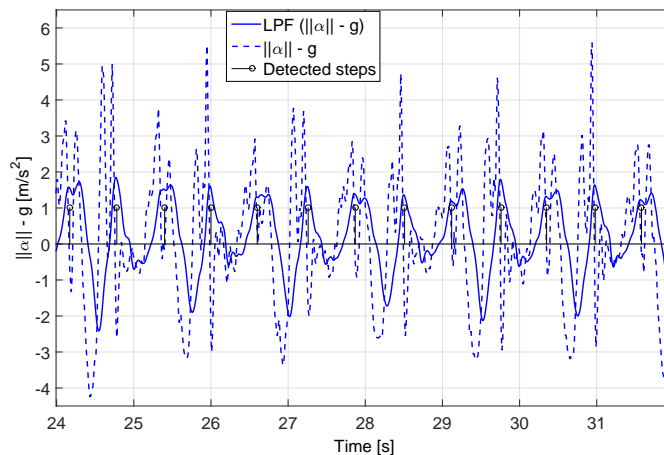


Figure 6: The dashed blue curve represents the norm of the acceleration $\|\alpha\|$ with the gravity compensated, while the solid blue curve represents the low-pass filtered (LPF) acceleration. The detected steps are highlighted with black sticks.

5.2. Step Detection on Stairs

255 Since the step&heading only based on inertial measurements is usually limited to horizontal displacements, i.e. 2D scenarios, the step detectors based on the acceleration do not offer reliable results when walking on stairs. The analysis carried out in [29] for 3D scenarios shows that the undetected steps rate is high. However, the false detection rate is dramatically reduced by using the

260 low-pass filtered acceleration. The authors in [29] concluded that it is possible to successfully detect all steps while walking on stairs with the pitch-based step detector. Figure 8 shows on the left side seven steps, where the first two steps were taken on an horizontal surface and the rest walking upstairs. The right side shows the pitch estimation during seven steps where the first four were

265 taken walking downstairs and on an horizontal surface and the following three walking horizontally. The authors in [29] show that detecting all steps is possible in 3D scenarios when using the pitch-based step detector. Additionally, it is possible to distinguish whether the pedestrian is walking horizontally, upstairs or downstairs, which is key to estimate the vertical displacement.

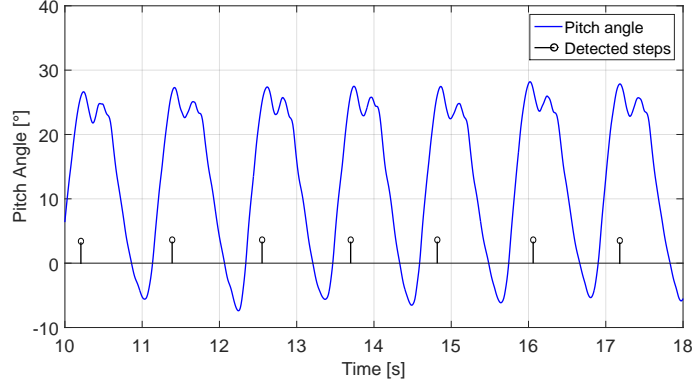


Figure 7: The blue curve represents the pitch angle estimation over seven steps and the steps detected are highlighted with black sticks.

270 5.3. Step Length Estimation

The main current algorithms to compute the step length s^k at each time k can be classified depending on the sensor location, as specified in [31, 32].

If the sensor is attached to the body near the center of mass, two options exists:

- Based on a biomechanical model, where the kneeless biped is modeled as an inverted pendulum. The final estimation is scaled by a constant m that is calibrated for each user [33].

$$s^k = m \cdot \sqrt{2 \cdot L \cdot d_{z_p}^k - d_{z_p}^k{}^2}, \quad (26)$$

275 where $d_{z_p}^k$ represents the vertical displacement of the pelvis at the time k and L , the leg's length.

- Using an empirical relationship of the vertical acceleration and the step length [34, 35]. The final estimation is scaled by a constant m that is calibrated for each user.

$$s^k = m \cdot \sqrt[4]{\alpha_{z_{\max}} - \alpha_{z_{\min}}}, \quad (27)$$

where $\alpha_{z_{\max}}$ and $\alpha_{z_{\min}}$ are the maximum and minimum values of the vertical acceleration during each step.

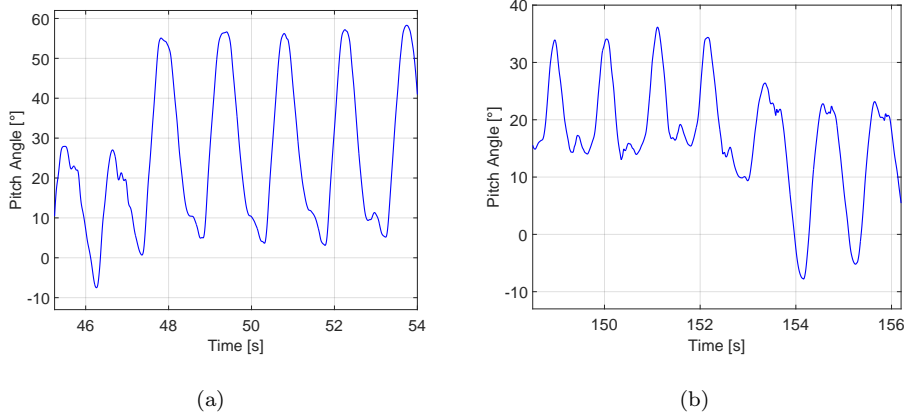


Figure 8: The left figure shows the pitch angle estimation when walking first two steps horizontally and then upstairs. The right figure shows the pitch angle estimation when walking downstairs and the last three steps were taken walking horizontally.

If there are no restrictions on the sensor location on the human body [36, 37, 38, 39, 40], taking advantage of the relationship between step length, height of the user h , step frequency f_s^k at the time k and the calibration parameters (j, l, q) different for each user, the step length can be estimated as:

$$s^k = h \cdot (j \cdot f_s^k + l) + q. \quad (28)$$

In [28], the step length estimator based on the pitch angle was presented. The authors assessed the relationship between the pitch amplitude and the step length with measurements recorded by 18 volunteers of different age, gender, height and weight at different walking speeds. The authors propose a linear step length model based as follows:

$$s^k = j \cdot \Delta\theta_H^k + l, \quad (29)$$

where $\Delta\theta_H^k$ represents the pitch amplitude in horizontal surfaces at the time k .

280 The parameters (j, l) can be universal or personalized for each pedestrian.

The authors in [29] show an analysis comparing the step length estimator based on the step frequency and based on the pitch angle for a sensor introduced in the front pocket of the trousers. The results reveal that, for normal and

constant walking speed, both estimators offer similar performance. However,
 285 for very low walking speed including stops and for high walking speeds, the
 detector based on the pitch angle offers more accurate results than the detector
 based on the step frequency.

5.4. Vertical Displacement Estimation

The authors in [29] estimate, for the first time, the vertical displacement in
 a step&heading algorithm using only inertial sensors. This is possible thanks
 to the pitch angle estimation that allows identifying whether the pedestrian is
 walking horizontally or climbing stairs. The pitch angle estimation allows also
 distinguishing between walking downstairs and upstairs. In order to estimate
 the vertical displacement d_v , the authors carried out a set of experiments with
 the objective of finding a relationship between the pitch angle and the height of
 the steps of the staircase. The results show that there is a relationship between
 the amplitude of the pitch angle and the height of the steps. The authors
 propose a linear model that relates these two variables for walking downstairs
 and upstairs as follows:

$$\begin{aligned} d_{v_U}^k &= j \cdot \Delta\theta_U^k + l, \\ d_{v_D}^k &= q \cdot \Delta\theta_D^k + w, \end{aligned} \tag{30}$$

where $d_{v_U}^k$ and $d_{v_D}^k$ are the estimated vertical displacement for up and down-
 290 stairs, respectively, at the time stamp k . $\Delta\theta_U^k$ and $\Delta\theta_D^k$ represent the pitch
 amplitude for steps up- and down, respectively, at the time stamp k . The pa-
 rameters (j, l, q, w) can be universal or personalized for each pedestrian.

The presented model is valid to estimate the height of the steps up and
 down of the vast majority of the staircases that can be found in every building,
 295 because it assumes a standard depth and focuses on the height of the step.
 Thus, the horizontal displacement is assumed.

Figure 9 shows a 3D trajectory corresponding to a walk recorded in the
 German museum in Munich with the sensor introduced in the front pocket of
 the trousers and using only inertial sensors. The walk starts at $(0, 0, 0)$ and at

300 the point (90, -20, 0) the pedestrian takes the stairs until the first floor. Then the pedestrian walks a round on the first floor and takes the stairs to the second floor. After some rounds on the second floor the pedestrian walks downstairs two floors and comes back to the initial position.

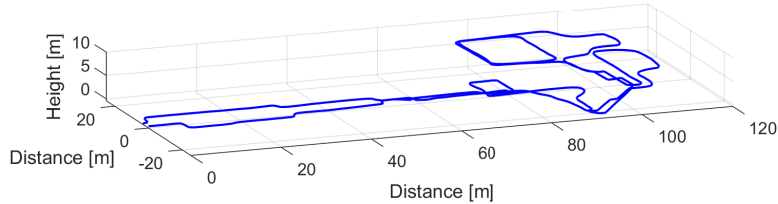


Figure 9: The blue curve shows the 3D trajectory estimated using only inertial sensors introduced in the front pocket of the trousers.

The algorithm proposed by the authors assumes that the height of all steps
 305 of the staircase is the same, i.e. v_U and v_D are equal. Thus, the algorithm gathers data when walking up- and downstairs and the height of the steps of the staircase is estimated with the average of the pitch amplitude of all steps up and down using Equation (30).

6. Drift Reduction Methods

310 Regarding pedestrian inertial navigation systems using medium- and low-cost MEMS sensors, the accumulated error in the yaw angle estimation is still an unsolved issue. This error, commonly called drift, should be computed and used to prevent positioning errors.

The authors in [19] concluded that the drift error is mainly composed of
 315 biases, particularly the bias of the z-axis gyroscope. The biases of the x- and y-axes gyroscopes can be estimated through the gravitational field, as assessed in [19]. Therefore, the error in roll and pitch angles can be corrected with the estimation of the x- and y-axes biases. On the contrary, the yaw angle suffers from ever growing errors that mainly arise from a poor estimation of the bias
 320 of the z-axis gyroscope [19].

Additionally, there is an accumulating error in the vertical axis, i.e. height error. This severe error is in most of the cases mitigated with the use of barometers. However, there are also solutions for only inertial-based systems that are described in this section.

325 6.1. Heuristic Drift Elimination Algorithms

Heuristic drift elimination algorithms assume that pedestrians walk on a straight line in the building in directions which are parallel to the outer walls of the building. If the pedestrian does not move on a straight line, these corrections are suspended [41]. After the first heuristic drift elimination algorithm
330 was published, many authors in the literature have proposed similar ideas or improvements, such as coping with complex buildings including curved corridors or wide areas not restricted by corridors [42, 43, 44].

Additionally, the heuristic drift elimination has been suggested in combination with other heading corrections such as zero angular rate updates and
335 magnetic measurements [45, 46]. The combination with available maps has also been proposed to restrict the possible heading angles by taking into account the walls of the buildings [47, 48]. The high non-linearities of the maps force the use of particle filters that weight the particles according to the similarity of their heading with the direction of the walls. The main drawback of these
340 approaches is that previous knowledge is necessary, e.g. the map or the shape of the corridors.

6.2. SLAM-Based Algorithms

A suitable solution to drift reduction is the use of the simultaneous localization and mapping (SLAM) algorithm, which has been used for decades in
345 robotics. The SLAM algorithm simultaneously generates a map of the desired landmarks and locates the user/robot within this map. These landmarks can be detected with any sensor, such as a laser scanner or a camera. The automatic vacuum cleaner, for example, generates a map of the room and locates itself

within this map where the interesting landmarks, i.e. sofa, table, doors, are
350 included.

The SLAM algorithm has also been adapted to pedestrian navigation aiming at reducing the drift error. In order for the SLAM algorithm to successfully reduce the drift, a re-visit is necessary. That means, the pedestrian detects landmarks during the trajectory and, when part of the trajectory is re-visited, the
355 landmark is again detected. The same landmark detected twice is an indicative of being again at the same position, therefore, corrections can be applied.

Commonly a particle filter is used that generates particles that move with different errors. When landmarks are re-visited, all particles are weighted depending on the landmarks position. Thus, particles that followed a trajectory
360 with the current drift are high weighted, because they most likely correspond to the detected position. In [49], the 2D space is divided into a grid of uniform and adjacent hexagons, which can be considered as landmarks. When the same hexagons are re-visited the aforementioned corrections are carried out. The same procedure is applied for 3D trajectories but dividing the volume into
365 hexagonal prisms with eight faces [50]. This procedure can also be applied if the hexagons are identified by the magnetic field intensity [51]. The main drawback of these algorithms is the complexity and processing time to manage the numerous hexagons or hexagonal prisms.

In [52], the proposed landmarks are some location-related activities carried
370 out by the pedestrian, such as sitting, lying or opening doors. Based on the assumption that these activities are always performed at the same place, their repeated detection leads to the aforementioned corrections. The main drawback of these methods is that the heading estimation is not explicitly corrected, just corrections on the position are applied.

375 *6.3. Multi-Inertial Sensor Fusion*

Multi-inertial sensor fusion combines two or more inertial sensors to reduce the drift in inertial positioning systems. Multi-inertial sensor fusion algorithms can be classified into two types: loose coupling and tight coupling.

Loose coupling algorithms combine the output of different inertial position-
380 ing systems. The aim is to generate a combined position estimation with less
drift than the individual position estimations. The authors in [53] propose
a loose coupling algorithm to combine the outputs of a shoe-mounted and a
pocket-mounted inertial sensors. The so-called smart update approach is fol-
lowed, i.e. the individual position estimations are combined favouring auto-
385 matically the one containing less drift. A novel metric, the quality factor, is
proposed to seamlessly identify which position estimation contains less drift.

Tight coupling algorithms target drift reduction by combining the raw data
from two or more inertial sensors. On the one hand, inertial sensor arrays can be
used to process all individual acceleration and turn rate measurements. In [54],
390 a maximum likelihood estimator combines the measurements from an array and
the authors state that the information gained is proportional to the square of
the array dimension. On the other hand, human biomechanics can also be used
to reduce the drift. The body mounted sensors in [55] are combined to reduce
the drift in a gait monitoring system. The authors use a kinematic leg model
395 to ensure that the motion is coherent with the biomechanical behaviour of the
leg.

6.4. Landmark-Based Algorithms

In [56], a study has been carried out concluding that landmarks play an im-
portant role for pedestrian navigation, therefore, it is recommendable to develop
400 methods to include landmarks information in pedestrian navigation systems.

One of the most intuitive ways of detecting landmarks during the trajectory
is using visual information. The chosen landmarks are tracked over time in
order to use this motion to constrain the drift. In [57], a stereo vision camera
is used to extract the optical information of the landmarks. The heuristic drift
405 elimination algorithms can also be seen as landmark-based algorithms, since
the manmade straight corridors can be interpreted as landmarks. The main
difference is that the landmarks of the heuristic drift elimination algorithms do
not need to be tracked over time.

In [58], an algorithm that makes use of detected ramps in buildings for
410 correcting the drift is presented. In the article, foot-mounted inertial sensors
are used and the position of the ramps of the target building is previously
known. Ramps are detected through the slope of the terrain and corrections
of the position of the pedestrian are applied. However, this approach does
not compute the drift value. Therefore, although the position is corrected, the
415 proposed approach does not bound the error of the yaw angle.

In [59, 60], the authors propose the use of landmarks to compensate the drift
error. The proposed landmarks are corners and stairs, thus, plentiful in indoor
environments. These landmarks are seamlessly detected using only inertial sen-
sors. The algorithm is based on re-visiting these landmarks in order to perform
420 corrections. The trajectory of the landmark during the re-visit can be fully or
partially overlapped or even with no overlap. The novelty of this contribution
relies on computing the drift value. This accumulated drift is fed back to the
orientation filter. This approach allows the yaw angle to be corrected and also
prevent future positioning errors due to a drifted yaw angle estimation. Ad-
425 ditionally, position corrections are also carried out. The authors recommend,
depending on the positioning system requirements, to perform these corrections
online, while the landmarks are re-visited, or offline, computing the overall drift
value and using it to post-process the recorded data.

6.5. Height Error Correction

430 The error in the height computation is the source of the confusion between
different floors. This error is usually mitigated using barometers. The barometer
sensor relates the change of height with the atmospheric pressure changes. The
height error is mainly affecting the shoe-mounted inertial systems, because the
step&heading approach is usually 2D defined.

435 There are several approaches for only inertial-based systems using medium-
and low-cost MEMS sensors to correct the height error. The authors in [61] use
the pitch angle of the foot to identify if the pedestrian is walking on horizontal
surfaces or climbing stairs. The authors in [62] apply an empirical threshold of

to assume that the user is walking horizontally and apply height corrections.
440 These corrections act keeping the height at the same value, when the pedestrian
is walking horizontally and only during the mid-stance phase (see Figure 4). The
authors in [63] apply also height constraints based on a finite state machine step
detector.

7. Conclusions

445 In this chapter a review of the methods applied for pedestrian positioning
using inertial sensors has been presented. Pedestrian inertial positioning is
usually derived in two different ways depending on the location of the sensor on
the human body: i) for shoe-mounted sensors the strapdown algorithm is used,
due to the possibility of perform re-calibrations at every step; ii) for the rest of
450 body locations the step&heading algorithm is preferred.

The big advantage of medium- and low-cost MEMS inertial sensors relies
on their low price, small size and widespread. Additionally, inertial positioning
constitutes an infrastructure-less positioning system. Their clear disadvantage,
however, is the remaining drift error on the estimated positioning.

455 There are many publications tackling the compensation of the drift error
resulting when using inertial sensors. Drift affects inertial positioning disre-
garding the body location where the sensor is mounted on. Nowadays the trend
is clearly pointing at sensor fusion. That means, combining the information of
all sensors available. Especially recommended is the fusion with satellite and ra-
460 dio positioning systems. The piloting method does not suffer from drift, unlike
the dead-reckoning method that propagates and accumulates error over time.
This chapter, however, is focused on inertial sensors, thus, a review of the latest
drift reduction methods using only inertial sensors is provided.

However, the current research on pedestrian inertial positioning is slowly
465 approaching a static stage. While the latest proposals on sensor fusion and
drift reduction algorithms greatly contribute to a more accurate positioning,
the fact is that the drift error is low-bounded by the sensor technology. The

breakthrough will be driven by the next generation of compact inertial sensors. In future, the inertial pedestrian dead-reckoning performed with the strapdown
470 algorithm will be possible disregarding the body location where the sensor is mounted on. The next generation of high-quality compact inertial sensors will eliminate the current strong need of performing constant re-calibrations by offering a more steady bias stability.

References

- 475 [1] H. Liu, H. Darabi, P. Banerjee, J. Liu, Survey of wireless indoor positioning techniques and systems, *IEEE Transactions on Systems, Man, and Cybernetics, Part C: Applications and Reviews* 37 (6) (2007) 1067–1080.
- [2] Y. Gu, A. Lo, I. Niemegeers, A survey of indoor positioning systems for wireless personal networks, *IEEE Communication Surveys and Tutorials*
480 11 (13-32) (2009) 1281–1293.
- [3] R. Harle, A survey of indoor inertial positioning systems for pedestrians, *Communications Surveys & Tutorials, IEEE* 15 (3) (2013) 1281–1293.
- [4] E. Munoz Diaz, A. L. Mendiguchia Gonzalez, F. de Ponte Müller, Standalone Inertial Pocket Navigation System, *IEEE/ION Position Location and Navigation Symposium (PLANS)*.
485
- [5] D. Bousdar, E. Munoz Diaz, S. Kaiser, Performance comparison of foot- and pocket-mounted inertial navigation systems, in: *7th International Conference on Indoor Positioning and Indoor Navigation*, 4-7 October, 2016, Madrid, Spain, 2016.
- 490 [6] L. Diez, A. Alfonso Bahillo, S. Bataineh, A. Masegosa, A. Perallos, Enhancing improved heuristic drift elimination for wrist-worn pdr systems in buildings, in: *Vehicular Technology Conference (VTC-Fall)*, 2016 IEEE 84th, 2016, pp. 1–5.

- [7] J. Windau, L. Itti, Walking compass with head-mounted imu sensor, in: 495 2016 IEEE International Conference on Robotics and Automation (ICRA), 2016, p. 55425547.
- [8] T. Do, R. Liu, C. Yuen, M. Zhang, U. Tan, Personal dead reckoning using imu mounted on upper torso and inverted pendulum model, *IEEE Sensors Journal* 16 (21) (2016) 76007608.
- 500 [9] V. Renaudin, M. Susi, G. Lachapelle, Step length estimation using hand-held inertial sensors, *Sensors (Basel)* 12 (7).
- [10] S. Beauregard, Widyawan, M. Klepal, Indoor PDR performance enhancement using minimal map information and particle filters, in: *Proceedings of the IEEE/ION Position Location and Navigation Symposium (PLANS)* 2008, Monterey, USA, 2008. 505
- [11] B. Krach, P. Robertson, Cascaded estimation architecture for integration of foot-mounted inertial sensors, in: *Proceedings of the IEEE/ION Position Location and Navigation Symposium (PLANS)* 2008, Monterey, USA, 2008.
- [12] O. Woodman, R. Harle, Pedestrian localisation for indoor environments, 510 in: *Proceedings of UbiComp 2008*, Seoul, South Korea, 2008.
- [13] S. Kaiser, M. Khider, M. Garcia Puyol, L. Bruno, P. Robertson, Map aided indoor navigation, In: *Indoor Wayfinding and Navigation*, H. Karimi, Taylor and Francis (2015) 107–140.
- [14] O. J. Woodman, An introduction to inertial navigation, Tech. rep., University of Cambridge. Computer Laboratory, uCAM-CL-TR-696 ISSN 1476- 515 2986 (August 2007).
- [15] J. Lenz, S. Edelstein, Magnetic sensors and their applications, *IEEE Sensors Journal* 6 (3) (2006) 631–649. doi:10.1109/JSEN.2006.874493.
- 520 [16] V. Beroulle, Y. Bertrand, L. Latorre, P. Nouet, Monolithic piezoresistive CMOS magnetic field sensors, *Sensors and Actuators A: Physical* 103 (1)

(2003) 23 – 32, micromechanics section of Sensors and Actuators, based on contributions revised from the Technical Digest of the 15th IEEE International conference on Micro Electro mechanical Systems (MEMS 2002). doi:[https://doi.org/10.1016/S0924-4247\(02\)00317-5](https://doi.org/10.1016/S0924-4247(02)00317-5).

525 URL <http://www.sciencedirect.com/science/article/pii/S0924424702003175>

[17] M. Azfal, V. Renaudin, G. Lachapelle, Use of Earth’s Magnetic Field for Mitigating Gyroscope Errors Regardless of Magnetic Perturbation, *Sensors* 11 (2011) 11390–11414.

530 [18] F. Zampella, M. Khider, P. Robertson, A. Jimenez, Unscented Kalman Filter and Magnetic Angular Rate Update (MARU) for an Improved Pedestrian Dead-Reckoning, *IEEE/ION Position Location and Navigation Symposium (PLANS)*.

[19] E. Munoz Diaz, F. de Ponte Müller, J. García Domínguez, Use of the magnetic field for improving gyroscopes’ biases estimation, *Sensors* 17 (2017) 832. doi:[10.3390/s17040832](https://doi.org/10.3390/s17040832).
535 URL <http://www.mdpi.com/1424-8220/17/4/832>

[20] J. Wagner, T. Wieneke, Integrating Satellite and Inertial Navigation - Conventional and New Fusion Approaches, *Control Engineering Practice* 11 (5) (2003) 543–550.
540

[21] E. Munoz Diaz, O. Heirich, M. Khider, P. Robertson, Optimal Sampling Frequency and Bias Error Modeling for Foot-Mounted IMUs, *IEEE International Conference on Indoor Positioning and Indoor Navigation (IPIN)*.

[22] V. Renaudin, C. Combettes, Magnetic, Acceleration Fields and Gyroscope Quaternion (MAGYQ)-Based Attitude Estimation with Smartphone Sensors for Indoor Pedestrian Navigation, *Sensors* 14 (2014) 22864–22890.
545

[23] J. B. Bancroft, G. Lachapelle, Use of Magnetic Quasi Static Field (QSF)

Updates for Pedestrian Navigation, IEEE/ION Position Location and Navigation Symposium (PLANS).

- 550 [24] P. Groves, Principles of GNSS, Inertial, and Multisensor Integrated Navigation Systems, 2nd ed, Artech House, 2013.
- [25] E. Foxlin, Pedestrian Tracking with Shoe-Mounted Inertial Sensors, IEEE Computer Graphics and Applications 25 (6) (2005) 38–46.
- [26] Streifeneder, The eight phases of human gait cycle, https://www.streifeneder.com/downloads/o.p./400w43_e_poster_gangphasen_druck.pdf (2016).
555
- [27] J. Ruppelt, N. Kronenwett, G. Scholz, G. F. Trommer, High-precision and robust indoor localization based on foot-mounted inertial sensors, in: 2016 IEEE/ION Position, Location and Navigation Symposium (PLANS), 2016, pp. 67–75. doi:10.1109/PLANS.2016.7479684.
560
- [28] E. Munoz Diaz, A. L. Mendiguchia Gonzalez, Step Detector and Step Length Estimator for an Inertial Pocket Navigation System, IEEE International Conference on Indoor Positioning and Indoor Navigation (IPIN).
- [29] E. Munoz Diaz, Inertial Pocket Navigation System: Unaided 3D Positioning, Sensors 15 (2015) 9156–9178. doi:10.3390/s150409156.
565 URL <http://www.mdpi.com/1424-8220/15/4/9156>
- [30] Z. Xiao, H. Wen, A. Markham, N. Trigoni, Robust Pedestrian Dead Reckoning (R-PDR) for Arbitrary Mobile Device Placement, IEEE International Conference on Indoor Positioning and Indoor Navigation (IPIN).
- 570 [31] D. Alvarez, R. C. González, A. López, J. C. Alvarez, Comparison of step length estimators from wearable accelerometer devices, in: Engineering in Medicine and Biology Society, 2006. EMBS'06. 28th Annual International Conference of the IEEE, IEEE, 2006, pp. 5964–5967.

- [32] J. Jahn, U. Batzer, J. Seitz, L. Patino-Studencka, J. Gutiérrez Boronat,
575 Comparison and evaluation of acceleration based step length estimators
for handheld devices, in: Indoor Positioning and Indoor Navigation (IPIN),
2010 International Conference on, IEEE, 2010, pp. 1–6.
- [33] W.-Y. Shih, L.-Y. Chen, K.-C. Lan, Estimating walking distance with a
smart phone, in: Parallel Architectures, Algorithms and Programming
580 (PAAP), 2012 Fifth International Symposium on, IEEE, 2012, pp. 166–
171.
- [34] Y. Jin, H.-S. Toh, W.-S. Soh, W.-C. Wong, A robust dead-reckoning pedes-
trian tracking system with low cost sensors, in: Pervasive Computing and
Communications (PerCom), 2011 IEEE International Conference on, IEEE,
585 2011, pp. 222–230.
- [35] P. Goyal, V. J. Ribeiro, H. Saran, A. Kumar, Strap-down pedestrian dead-
reckoning system, in: Indoor Positioning and Indoor Navigation (IPIN),
2011 International Conference on, IEEE, 2011, pp. 1–7.
- [36] S. Shin, M. Lee, C. Park, H. S. Hong, Pedestrian dead reckoning system
590 with phone location awareness algorithm, in: Position Location and Navi-
gation Symposium (PLANS), 2010 IEEE/ION, IEEE, 2010, pp. 97–101.
- [37] D. Gusenbauer, C. Isert, J. Krosche, Self-contained indoor positioning on
off-the-shelf mobile devices, in: Indoor Positioning and Indoor Navigation
(IPIN), 2010 International Conference on, IEEE, 2010, pp. 1–9.
- [38] V. Renaudin, V. Demeule, M. Ortiz, Adaptive pedestrian displacement
595 estimation with a smartphone, international Conference on Indoor Posi-
tioning and Indoor Navigation 12 (2013) 916–924.
- [39] S. Shin, C. Park, J. Kim, H. Hong, J. Lee, Adaptive step length estimation
algorithm using low-cost mems inertial sensors, in: Sensors Applications
600 Symposium, 2007. SAS’07. IEEE, IEEE, 2007, pp. 1–5.

- [40] V. Renaudin, M. Susi, G. Lachapelle, Step length estimation using hand-held inertial sensors, *Sensors* 12 (7) (2012) 8507–8525.
- [41] J. Borenstein, L. Ojeda, Heuristic Drift Elimination for Personnel Tracking Systems, *The Royal Institute of Navigation* 63 (2010) 591–606.
- 605 [42] K. Abdulrahim, C. Hide, T. Moore, C. Hill, Aiding MEMS IMU with Building Heading for Indoor Pedestrian Navigation, *Ubiquitous Positioning Indoor Navigation and Location Based Service (UPINLBS)*.
- [43] K. Abdulrahim, C. Hide, T. Moore, C. Hill, Using Constraints for Shoe Mounted Indoor Pedestrian Navigation, *The Royal Institute of Navigation*
610 65 (2012) 15–28.
- [44] A. R. Jimenez, F. Seco, F. Zampella, J. C. Prieto, Improved Heuristic Drift Elimination (iHDE) for Pedestrian Navigation in Complex Buildings, *IEEE International Conference on Indoor Positioning and Indoor Navigation (IPIN)* (2011) 1–8.
- 615 [45] A. R. Jimenez, F. Seco, J. C. Prieto, J. Guevara, Indoor Pedestrian Navigation Using an INS/EKF Framework for Yaw Drift Reduction and a Foot-Mounted IMU, *7th Workshop on Positioning Navigation and Communication (WPNC)* (2010) 135–143.
- [46] A. R. Jimenez, F. Seco, F. Zampella, J. C. Prieto, J. Guevara, Improved
620 Heuristic Drift Elimination with Magnetically-Aided Dominant Directions (MiHDE) for Pedestrian Navigation in Complex Buildings, *Journal of Location Based Services* 6 (2012) 186–210.
- [47] P. Aggarwal, D. Thomas, J. Borenstein, L. Ojeda, Map Matching and Heuristic Elimination of Gyro Drift for Personal Navigation Systems in
625 GPS-Denied Conditions, *Journal of Measurement Science and Technology* 22.
- [48] J. Pinchin, C. Hide, T. Moore, A Particle Filter Approach to Indoor Navigation Using a Foot-Mounted Inertial Navigation System and Heuristic

- Heading Information, IEEE International Conference on Indoor Position-
630 and Indoor Navigation (IPIN) (2012) 1–10.
- [49] P. Robertson, M. Angermann, B. Krach, Simultaneous Localization and Mapping for Pedestrians using only Foot-Mounted Inertial Sensors, International Conference on Ubiquitous Computing (2009) 93–96.
- [50] M. Garcia Puyol, D. Bobkov, P. Robertson, T. Jost, Pedestrian Simultaneous Localization and Mapping in Multistory Buildings Using Inertial Sensors, IEEE Transactions on Intelligent Transportation Systems 15 (2014) 635 1714–1727.
- [51] P. Robertson, M. Frassl, M. Angermann, M. Doniec, B. J. Julian, M. Garcia Puyol, M. Khider, M. Lichtenstern, L. Bruno, Simultaneous Localization and Mapping for Pedestrians Using Distortions of the Local magnetic Field Intensity in Large Indoor Environments, IEEE International Conference on Indoor Positioning and Indoor Navigation (IPIN) (2013) 1–10. 640
- [52] M. Hardegger, D. Roggen, S. Mazilu, G. Troster, ActionSLAM: Using location-related Actions as Landmarks in Pedestrian SLAM, IEEE International Conference on Indoor Positioning and Indoor Navigation (IPIN). 645
- [53] D. Bousdar Ahmed, E. Munoz Diaz, Loose Coupling of Wearable-Based INs with Automatic Heading Evaluation, Sensors 17 (2017) 2534. doi: 10.3390/s17112534.
URL <http://www.mdpi.com/1424-8220/17/11/2534>
- [54] I. Skog, J.-O. Nilsson, P. Handel, A. Nehorai, Inertial sensor arrays, maximum likelihood, and cram-rao bound, IEEE Transactions on Signal Processing 64 (16) (2016) 4218–4227. doi:10.1109/tsp.2016.2560136. 650
- [55] A. Ahmadi, F. Destelle, D. Monaghan, K. Moran, N. E. O-Connor, L. Unzueta, M. T. Linaza, Human Gait Monitoring Using Body-Worn Inertial Sensors and Kinematic Modelling, in: 2015 IEEE SENSORS, IEEE, 2015. doi:10.1109/icsens.2015.7370310. 655

- [56] A. Millonig, K. Schechtner, Developing Landmark-Based Pedestrian-Navigation Systems, *IEEE Transactions on Intelligent Transportation Systems* 8 (1).
- 660 [57] D. Griesbach, D. Baumbach, S. Zuev, Stereo-Vision-Aided Inertial Navigation for Unknown Indoor and Outdoor Environments, *IEEE International Conference on Indoor Positioning and Indoor Navigation (IPIN)* (2014) 709–716.
- [58] A. Jimenez R., F. Seco, F. Zampella, J. C. Prieto, J. Guevara, PDR with
665 a Foot-Mounted IMU and Ramp Detection, *Sensors* 11 (2011) 9393–9410.
- [59] E. Munoz Diaz, M. Caamano, F. Fuentes Sanchez, Landmark-Based Drift Compensation Algorithm for Inertial Pedestrian Navigation, *Sensors* 17 (2017) 1555. doi:10.3390/s17071555.
URL <http://www.mdpi.com/1424-8220/17/7/1555>
- 670 [60] E. Munoz Diaz, M. Caamano, Landmark-Based Online Drift Compensation Algorithm for Inertial Pedestrian Navigation, *IEEE International Conference on Indoor Positioning and Indoor Navigation (IPIN)*.
- [61] E. Munoz Diaz, S. Kaiser, D. Bousdar Ahmed, Height Error Correction for Shoe-Mounted Inertial Sensors Exploiting Foot Dynamics, *Sensors* 18
675 (2018) 888. doi:10.3390/s18030888.
URL <http://www.mdpi.com/1424-8220/18/3/888>
- [62] K. Abdulrahim, C. Hide, T. Moore, C. Hill, Using Constraints for Shoe Mounted Indoor Pedestrian Navigation, *Journal of Navigation* 65 (2012) 15–28.
- 680 [63] J. Ruppelt, N. Kronenwett, G. Scholz, G. Trommer, High-Precision and Robust Indoor Localization Based on Foot-Mounted Inertial Sensors, *IEEE/ION Position Location and Navigation Symposium (PLANS)* (2016) 67–75.